Determination of the Metal–Hydrogen and Metal–Methyl Bond Dissociation Energies of the Second-Row, Group 8 Transition Metal Cations

M. L. Mandich, L. F. Halle, and J. L. Beauchamp*

Contribution No. 6909 from the Arthur Amos Noyes Laboratory of Chemical Physics, California Institute of Technology, Pasadena, California 91125. *Received December 19, 1983*

Abstract: The gas-phase reactions of three metal ions, Ru^+, Rh^+, and Pd^+, with dihydrogen and ethane are studied in an ion beam apparatus as a function of relative kinetic energy. Analysis of the thresholds for the endothermic formation of metal–hydrogen ions in the reaction with dihydrogen yields the bond dissociation energies $D°(Ru^+–H) = 41 \pm 3$ kcal/mol, $D°(Rh^+–H) = 42 \pm 3$ kcal/mol, and $D°(Pd–H) = 45 \pm 3$ kcal/mol. Similarly, analysis of the thresholds for the endothermic formation of metal–methyl ions in the reaction with ethane yields the bond dissociation energies $D°(Ru^+–CH_3) = 54 \pm 5$ kcal/mol, $D°(Rh^+–CH_3) = 47 \pm 5$ kcal/mol, and $D°(Pd^+–CH_3) = 59 \pm 5$ kcal/mol. The periodic trends for these bond energies are modeled semiquantitatively using simple covalent and electrostatic bonding models. The results of these model calculations indicate that the increased $M^+–CH_3$ bond strength relative to the $M^+–H$ bond is most likely caused by a resonant charge stabilization of the metal cation by the methyl ligand. Almost certainly for Ru, Rh, and Pd these $M^+–R$ bonds are predominately covalent in character with the metal contribution to the bond being mostly d-like. Contributions from $M^{2+}–R^-$ type structures appear to be unimportant.

Introduction

Bond dissociation energies provide a basis for predicting stable molecular structures, designing rational syntheses, proposing reaction mechanisms, and testing theoretical chemical bonding models. Although bond strengths have been measured and calculated for a great many organic species, the number of bond strengths known for organometallic moieties is extremely limited.[1,2] By far the most useful quantity is the dissociation energy of a *particular* metal–ligand bond as opposed to an *average* over several metal–ligand bond energies. Calorimetric measurements generally yield only the latter quantities.[1] Determination of activation parameters in thermochemical kinetic studies and the direct use of spectroscopic methods have provided limited results for individual metal–ligand bond dissociation energies.[3-5] One method whereby a single metal ligand bond can be isolated for study is to examine an appropriate organometallic fragment which has no other ligands attached. Even though these species are coordinatively unsaturated and may not directly resemble isolatable organometallics, they permit the desired thermochemical studies while facilitating the development of theoretical models for describing metal–ligand bonds.

Ion beam reactive scattering methods afford a means of studying the reactions of metal ions with neutral molecules to form organometallic fragments. By adjusting the relative kinetic energy, the threshold energy for formation of a particular organometallic bond can be ascertained, leading to a direct measure of the dissociation energy of that bond. This experimental methodology can also provide thermochemical data for neutral fragments,[6,7] but they have been less extensively investigated. In this work, we use these techniques to determine the metal–hydrogen and metal–methyl bond dissociation energies for Ru^+, Rh^+, and Pd^+. A comparison of our results to the predictions of simple covalent and electrostatic bonding models serves to highlight the importance of metal d-orbital covalency in these second-row, group 8 transition metals. The reactions of Ru^+, Rh^+, and Pd^+ with simple hydrocarbons have also been studied and will be reported elsewhere.[8]

Table I. Lower Electronic States of Ru^+, Rh^+, and Pd^+ and Their Relative Ion Populations at 2500 K[a]

	state[b]	energy[c] (eV)	rel ion population, %
Ru^+	$X^4F(4d^7)$	0.18	99
	^4P	1.06	1
	$^6D(4d^65s^1)$	1.27	<1
	^2G	1.43	~0
	^2P	1.68	~0
	^2D	1.93	~0
Rh^+	$X^3F(4d^8)$	0.20	>99
	^1D	1.01	0.4
	^3P	1.38	<0.1
	^1G	1.84	~0
	^5F	2.33	~0
	$^3F(4d^75s^1)$	3.33	~0
Pd^+	$X^2D(4d^9)$	0.18	100
	$^4F(4d^85s^1)$	3.37	<<0.01
	$^2F(4d^85s^1)$	4.12	~0
	$^4P(4d^85s^1)$	4.59	~0
	$^2D(4d^85s^1)$	5.03	~0
	$^2P(4d^85s^1)$	5.42	~0

[a] The ground electronic states are prefixed with an "X". [b] All states are $4d^n$ configurations unless otherwise denoted. [c] State energies cited are averaged over J states from ref 16.

Experimental Section

A description of the ion beam apparatus used for these experiments is available elsewhere.[9,10] Ions were generated either by electron impact or surface ionization. The surface ionization source[10,11] was used to produce Ru^+, Rh^+, and Pd^+ from $Ru_3(CO)_{12}$, $[Rh(CO)_2Cl]_2$, and $PdCl_2$(anhy). These inorganic chemicals were obtained from Alfa Products and used without further purification. Production of Ru^+, Rh^+, and Pd^+ beams proved to be considerably more difficult than beams of

(1) J. A. Connor, *Top. Curr. Chem.*, **71**, 71 (1977).
(2) P. B. Armentrout, L. F. Halle, and J. L. Beauchamp, *J. Am. Chem. Soc.*, **103**, 6501 (1981).
(3) K. P. Huber and G. Herzberg, "Molecular Spectra and Molecular Structure. IV. Constants of Diatomic Molecules", Van Nostrand Reinhold, New York, 1979.
(4) "JANAF Tables", *J. Phys. Chem. Ref. Data*, **4** (1975).
(5) A. G. Gaydon, "Dissociation Energies and Spectra of Diatomic Molecules", Chapman and Hall, London, 1968.
(6) L. F. Halle, P. B. Armentrout, and J. L. Beauchamp, *J. Am. Chem. Soc.*, **103**, 962 (1981).
(7) L. F. Halle, F. S. Klein, and J. L. Beauchamp, to be submitted for publication.
(8) M. L. Mandich and J. L. Beauchamp, "The Reactions of the Second Row Group VIII Transition Metal Cations with Simple Hydrocarbons in an Ion Beam," to be submitted for publication.
(9) P. B. Armentrout, R. V. Hodges, and J. L. Beauchamp, *J. Chem. Phys.*, **66**, 4683 (1977).
(10) P. B. Armentrout and J. L. Beauchamp, *J. Chem. Phys.*, **74**, 2819 (1981).
(11) P. B. Armentrout and J. L. Beauchamp, *J. Am. Chem. Soc.*, **103**, 784 (1981).

0002-7863/84/1506-4403$01.50/0

Table II. Values of the Threshold Energy, E_0, and Energy-Independent Cross Section, σ_0, for the Reaction $M^+ + D_2 \rightarrow MD^+ + D$

M^+	E_0 (eV)	σ_0 (Å^2)
Ru^+	2.82	13
Rh^+	2.67	2
Pd^+	2.65	4

Table III. Values of the Threshold Energy, E_0, Energy-Independent Cross Section, σ_0, Number of Equilibrated Degrees of Freedom, n, and Fraction of Internal Energy Retained in the Product, a, for the Reaction[a] $M^+ + C_2D_6 \rightarrow MCD_3^+ + CD_3$

M^+	E_0 (eV)	σ_0 (Å^2)	n	a
Ru^+	1.56	11	5	0.9
Rh^+	1.85	9	4	0.8
Pd^+	1.34	10	4	0.9

[a] For a detailed discussion of the meaning of n and a in these data, see ref 3.

Table IV. Summary of Group 8 Metal–Ligand Bond Dissociation Energies (kcal/mol)

R	Fe^+–R	Co^+–R	Ni^+–R
H	58 ± 5	52 ± 4	43 ± 2
CH_3	68 ± 4	61 ± 4	48 ± 5
R	Ru^+–R	Rh^+–R	Pd^+–R
H	41 ± 3	42 ± 3	45 ± 3
CH_3	54 ± 5	47 ± 5	59 ± 5

first-row transition metal ions.[2,10,11] Evaporation of the simple transition metal halide salt was successful in only one instance, $PdCl_2$, and required that the salt be anhydrous. The two precursors used for Rh^+ and Ru^+ were arrived at by trial and error. In all cases, extensive plating of the source region occurred after a relatively short time, and the duration of an experiment depended on how quickly various electrical insulators became metal coated. The temperature of the ionizing filament in these experiments was about 2500 K. Assuming that the ions are also described by this temperature, the relative populations of the electronic states of Ru^+, Rh^+, and Pd^+ can be estimated by applying the Boltzmann distribution law to the known electronic state energies.[12] As shown in Table I, this calculation suggests that the ion beam reactions observed are due to ground-state metal cations. The typical spread in ion beam kinetic energy for these experiments was between 0.5 and 1.0 eV (fwhm) as measured with a retarding field energy analyzer. This uncertainty contributes very little to the center-of-mass energy spread, however, where it introduces an error of ±0.01–0.02 eV for D_2 and ±0.13–0.07 eV for C_2D_6 target gases.

Several experiments with Rh^+ were performed using an electron impact ion source[7] to create Rh^+ as a fragment ion from the volatile liquid, $(\eta^5\text{-}C_5H_5)Rh(CO)_2$. This chemical was synthesized as described in the literature[13] and purified by distillation. The internal state distributions of ions from the electron impact source are poorly described.[3] Usable beam intensities required electron impact energies in excess of 20 eV, which is sufficient to produce electronically excited Rh^+.

Results

Product cross sections measured as a function of translational energy for reactions 1 and 2 (where M = Ru, Rh, and Pd) are

$$M^+ + D_2 \rightarrow MD^+ + D \quad (1)$$

$$M^+ + C_2D_6 \rightarrow MCD_3^+ + CD_3 \quad (2)$$

shown in Figures 1 and 2, respectively.[14] Thorough discussions

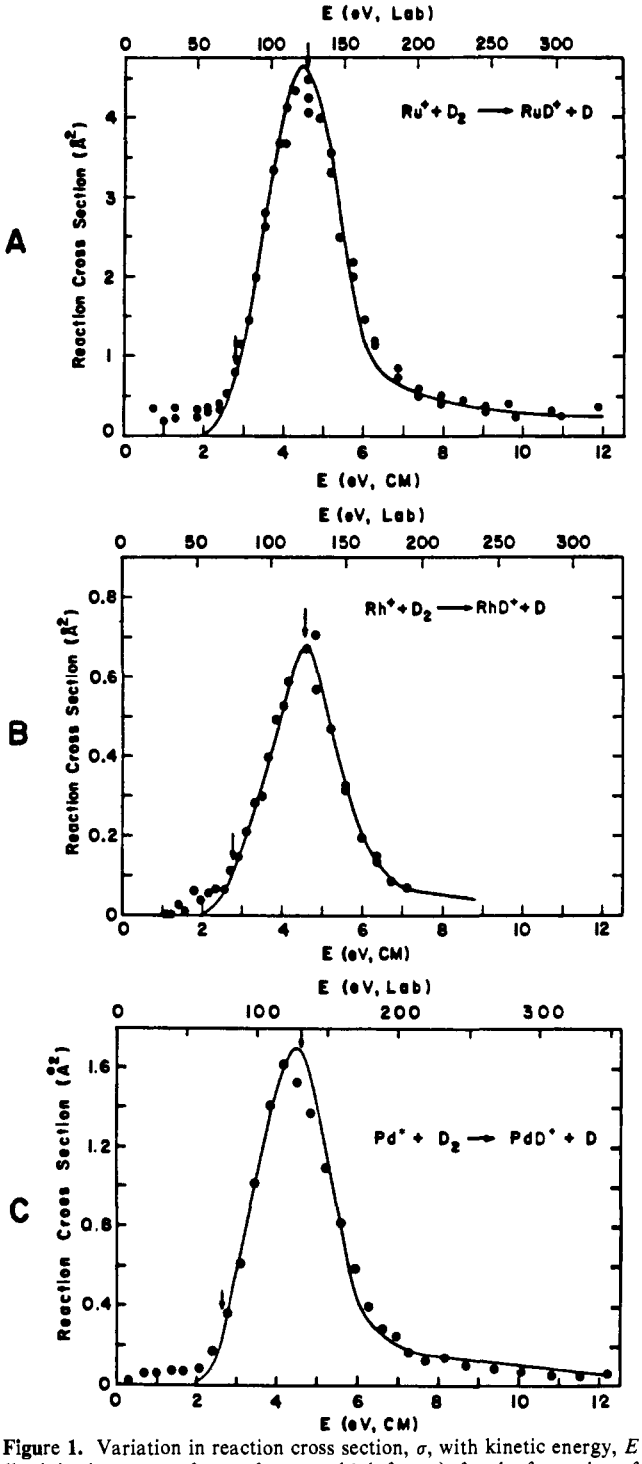

Figure 1. Variation in reaction cross section, σ, with kinetic energy, E (both in the center-of-mass frame and lab frame), for the formation of MD^+ from the reaction of M^+ with D_2: (A) M = Ru, (B) M = Rh, and (C) M = Pd. The curves drawn through the data sets A–C are derived from a theoretical analysis as discussed in the text. Arrows indicate the D_2 bond energy of 4.6 eV and the threshold energies for reaction at 2.82 (Ru), 2.67 (Rh), and 2.65 eV (Pd). All of the M^+ were produced by surface ionization.

of the assumptions and theoretical models used to analyze the data appear elsewhere.[10,15] Results of these analyses are given in Tables II and III. Errors cited for the threshold energies, E_0, in these tables reflect the sensitivity of the fitting parameters to the experimental data. Bond dissociation energies ($D°$) for MD^+ and MCD_3^+ are determined as differences between the threshold

(12) C. E. Moore, "Atomic Energy Levels", National Bureau of Standards, Washington, D.C., 1971.
(13) E. O. Fischer and K. Z. Bittler, *Z. Naturforsch. B*, **16**, 225 (1961).
(14) Although there are stoichiometrically equivalent structures for M^+—CH_3, such as $[H—M=CH_2]^+$ and $[H_2M\equiv CH]^+$, the experimental evidence favors the metal-methyl assignment. For example, where the $[M=CH_2]^+$ bond strengths are known, the $[H—M=CH_2]^+$ structure can be eliminated on the basis of energetics. Also, $[M—CH_3]^+$ bond strengths exceed $[M—H]^+$ bond strengths by 2–20 kcal for every M^+ studied, independent of the factors which would appear to promote alternate structures for certain M^+. See ref 2 for further discussion.
(15) P. B. Armentrout and J. L. Beauchamp, *Chem. Phys.*, **48**, 315 (1980), and references within.

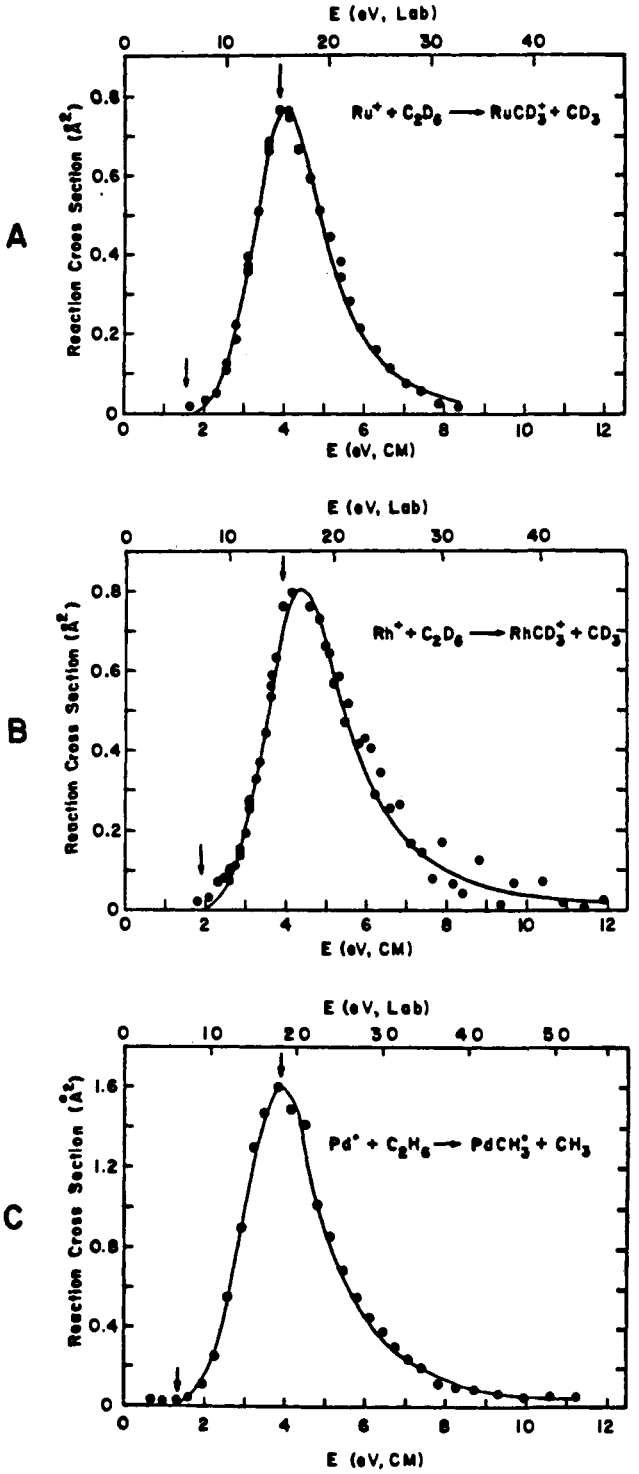

Figure 2. Variation in reaction cross section, σ, with kinetic energy, E (both in the center-of-mass frame and the lab frame), for the formation of MCD_3^+ (or MCH_3^+) from the reaction of M^+ with C_2D_6 (or C_2H_6): (A) M = Ru, (B) M = Rh, and (C) M = Pd. The curves drawn through the data sets A–C are derived from a theoretical analysis as discussed in the text. Arrows indicate the C–C bond energy in ethane of 3.9 eV and the threshold energies for reaction at 1.56 (Ru), 1.85 (Rh), and 1.34 eV (Pd). All of the M^+ were produced by surface ionization.

energy, E_0, and the energy of the bond broken in the neutral reagent as given in eq 3 (where R = D or CD_3) using $D°(D_2)$ =

$$D°(M^+\text{–R}) = D°(\text{R–R}) - E_0 \qquad (3)$$

4.6 eV and $D°(CD_3\text{–}CD_3)$ = 3.9 eV. A summary of these bond dissociation energies is given in Table IV. Note that the energetic differences between either MCH_3^+ and MCD_3^+ or MD^+ and MH^+ bond dissociation energies are negligible and they are often quoted interchangeably.

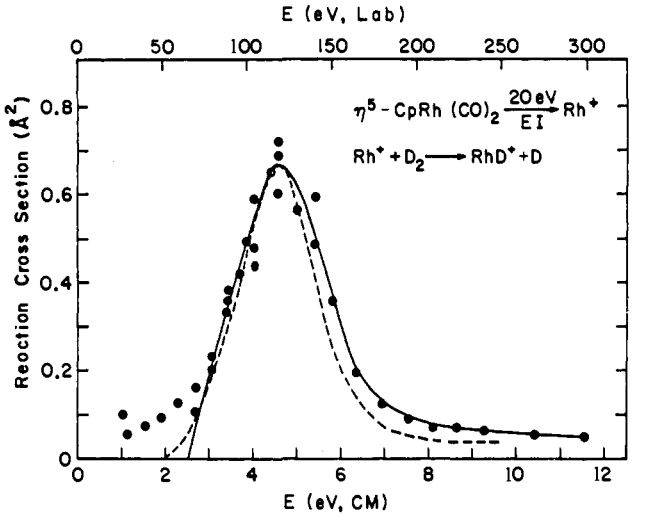

Figure 3. Variation in reaction cross section, σ, with kinetic energy, E (both in the center-of-mass frame and the lab frame) for the formation of RhD^+ in the reaction of Rh^+ with D_2 where the Rh^+ is formed as a fragment ion by electron impact on η^5-$CpRh(CO)_2$. The solid curve through the data points was derived using the theoretical analysis discussed in the text. The results for the $Rh^+ + D_2$ reaction where the Rh^+ ions are created by surface ionization (see Figure 1B) are shown by the dashed line for comparison.

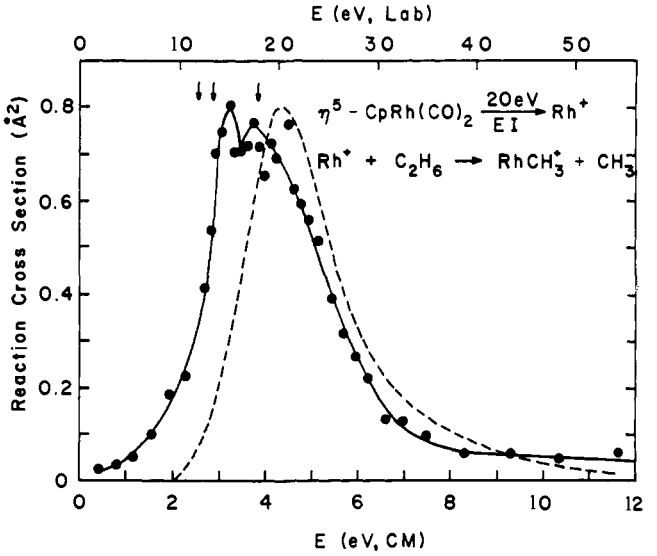

Figure 4. Variation in reaction cross section, σ, with kinetic energy, E (both in the center-of-mass frame and the lab frame) for the formation of $RhCH_3^+$ in the reaction of Rh^+ with C_2H_6 where the Rh^+ is formed as a fragment ion by electron impact on η^5-$CpRh(CO)_2$. The solid curve through the data points has not been derived from a theoretical model and is given only as a guide to indicate the dip in the data at about 3.6 eV which is quite reproducible. Arrows indicate the C–C bond energy of C_2H_6 at 3.9 eV and this C–C bond energy less the energy of Rh^+ excited into its first two lower states (which lie at about 1.0 and 1.4 eV). The dashed curve represents the data for this reaction where the Rh^+ ions have been created by surface ionization (see Figure 2B; a slight energy scaling of this data has been made so as to compare the reaction with C_2D_6 to that with C_2H_6).

Reactions 1 and 2 were also studied using a Rh^+ beam generated by 20-eV electron impact ionization of $(\eta^5\text{-}C_5H_5)Rh(CO)_2$. These results are compared with those obtained using the surface ionization source in Figures 3 and 4. While the data for reactions with D_2 are similar, distinct differences in reactivity are observed for C_2D_6. No thermochemical data were derived from the electron impact studies.

Discussion

Effect of Electronic Excitation in Promoting Reactions of Rh^+ with D_2 and C_2D_6. The efficacy of internal excitation in promoting

Table V. Summary of Bond Dissociation Energies of M^+–CH_3 and M^+–H (kcal/mol)

	Sc^+ [a]	Ti^+ [b]	V^+ [c,d]	Cr^+ [e]	Mn^+ [f]	Fe^+ [g]	Co^+ [e]	Ni^+ [e]	Cu^+ [d]	Zn^+ [h]
H	54 ± 4	60	50	35 ± 4	53 ± 3	59 ± 5	52 ± 4	43 ± 2	30	60
CH_3	65 ± 5	65		37 ± 7	71 ± 7	69 ± 5	61 ± 4	48 ± 5		67 ± 1

[a] Reference 18. [b] Reference 19. [c] Reference 20. [d] Reference 21. [e] Reference 2 and references therein. [f] These values are somewhat uncertain owing to difficulties in interpretation of the data; the results for MnH^+ agree within experimental error with those reported in ref 22. [g] See ref 23 for Fe^+–H and ref 7 for Fe^+–CH_3. [h] See ref 24 for Zn^+–H and ref 25 for Zn^+–CH_3.

elementary reactions has been increasingly studied by molecular and ion beam techniques.[6,16,17] Of the various possible forms of internal excitation, the fundamental effects of added electronic energy have been the least well characterized. While the straightforward interpretation of our experiments to determine bond dissociation energies demands that we use a ground-state metal ion beam, we are also able to infer that electronic excitation modifies the reactivity of Rh^+ with C_2D_6. The enhancement of $RhCD_3^+$ formation at low energies in Figure 4 is attributed to reaction of excited-state Rh^+ generated in the electron impact process. The threshold is lowered by about 1 eV, which may implicate the presence of Rh^+ excited to states of this energy such as ^1D and ^3P (Table I). Interestingly, the presence of excited Rh^+ does not appear to modify reactivity with D_2. This is in contrast to the behavior observed for the reaction of electronically excited Cr^+ with D_2, where the threshold was shifted to lower energy and the cross section was substantially increased.[6] Clearly, it would be of interest to pursue studies such as these in the future with a state-selected ion beam. One goal would be to distinguish whether the electronic excitation serves to augment merely the *total* available energy along the reaction coordinate or to provide an electronic configuration which can proceed to the product channel via a lower energy transition state. Finally, these results further underline the importance of exercising caution when analyzing the results of metal ion–molecule reactions in which the ions are formed by methods that are known to produce excited states, e.g., electron impact ionization and laser desorption ionization.

Periodic Trends in the Bond Dissociation Energies of Ru^+, Rh^+, and Pd^+ with D and CD_3. The data base for metal cation–ligand bond dissociation energies for hydrogen and methyl encompasses nearly the entire first row[2] (Table V) as well as the three group 8, second-row transition metal cations (Table IV). In the following discussion, the bond strength trends of Ru^+, Rh^+, and Pd^+ are examined, compared with simple theoretical models, and then compared with the data for the first-row transition metal cations. The calculations presented here model covalent and electrostatic metal–ligand bonds. Our intent is to have a "hands-on" approach in quantitatively predicting bond strength trends for these M^+–R systems. Further development of these ideas would be best accomplished by more sophisticated full ab initio or semiempirical theoretical treatments.[26]

One of the more intriguing trends observed for both the first- and second-row gas-phase transition metal cations is that, in every case studied, the metal–methyl bond is *stronger* than the metal–hydrogen bond by ~2–20 kcal/mol. This trend differs distinctly from that known for coordinatively saturated organometallic compounds where, with metals for which both values are known, metal–hydrogen bonds are 50–60 kcal/mol and the corresponding metal–methyl bonds are ~15 kcal/mol weaker.[27] The most probable origin of this difference between the M^+–R and saturated organometallic results is the coordinative unsaturation of the gas-phase M^+–R system. The absence of additional ligands around the gaseous M^+–R fragments precludes steric weakening of the metal ligand–bond and promotes the importance of polarization stabilization by the ligand of the highly acidic metal center (the latter is depicted in structure I; the +/− refer to electric charges).

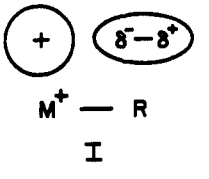

I

The relative stabilization of the metal center by the methyl vs. the hydrogen group is considered in section 1 of the following discussion using a model to evaluate the M^+–R interaction in which the metal ion induces a dipole on the ligand.

While ion-dipole forces are probably important in determining the relative strengths of metal–alkyl bonds for the M^+–R fragments, they are too weak to account for the overall bonding, and either covalent or ionic (acid–base) forces are expected to predominate. In sections 2 and 3 of the following discussion, we model both a covalent-type and ion-pair-type $(M–R)^+$ bond, respectively. The crucial test of these two concepts is their ability to reproduce, for Ru^+, Rh^+, and Pd^+, the experimental result that the M^+–H

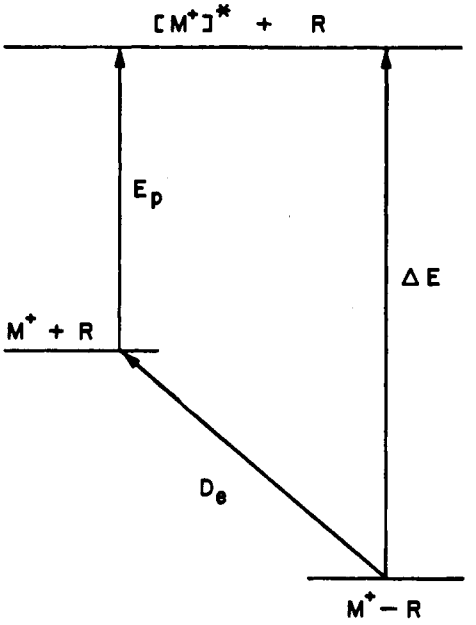

Figure 5. Schematic showing that the covalently bound M^+–R molecule consists of the union of a higher energy $[M^+]^*$ configuration with R. Thus, the resulting bond energy, D_e, equals the principal bond energy, ΔE, minus the energy required to prepare the $[M^+]^*$ configuration, E_p.

(16) R. B. Bernstein, "Chemical Dynamics via Molecular Beam and Laser Techniques", Oxford University Press, New York, 1982, pp 142–195.
(17) K. Tanaka, T. Kato, P. M. Guyon, and I. Koyano, *J. Chem. Phys.*, 79, 4302 (1983).
(18) M. A. Tolbert and J. L. Beauchamp, work in progress.
(19) J. B. Schilling, W. A. Goddard III, and J. L. Beauchamp, work in progress.
(20) P. B. Armentrout et al., work in progress.
(21) F. S. Klein and J. L. Beauchamp, unpublished results.
(22) A. E. Stevens and J. L. Beauchamp, *Chem. Phys. Lett.*, 78, 291 (1981).
(23) L. F. Halle, P. B. Armentrout, and J. L. Beauchamp, *Organometallics*, *1*, 963 (1982).
(24) P. L. Po, T. P. Radus, and R. F. Porter, *J. Phys. Chem.*, 82, 520 (1980).
(25) G. Distefano and V. H. Dibeler, *Int. J. Mass Spectrom. Ion Phys.*, *4*, 59 (1970).
(26) For an exhaustive review of this subject, see W. H. Miller, H. F. Schaefer, III, B. J. Berne, and G. A. Segal, Eds., "Methods of Electronic Structure Theory", Plenum Press, New York, 1977.
(27) J. A. Martinho Simões and J. L. Beauchamp, to be submitted for publication.

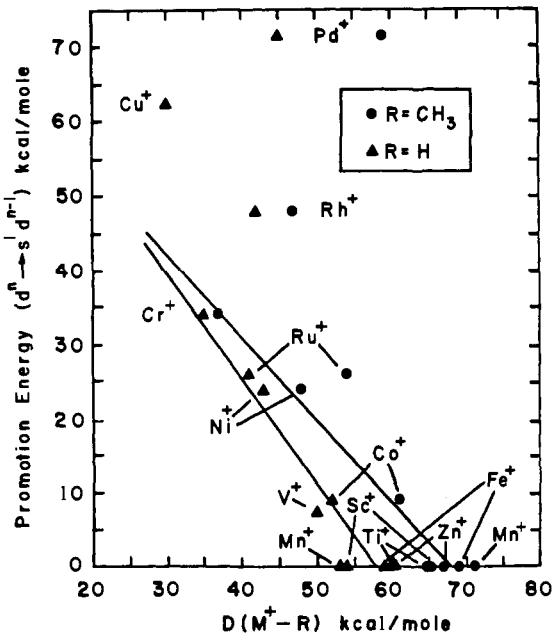

Figure 6. Plot of the measured M^+–R bond dissociation energy vs. the promotion energy required to prepare the M^+ in the lowest energy s^1d^{n-1} configuration. Note that for those metal ions which have a s^1d^{n-1} ground state, e.g., Mn^+, Ti^+, this promotion energy equals zero. This promotion energy is a very crude estimate for E_p (see Figure 5 and the text) where the bonding electron on the metal is presumed to be entirely s in character.

bonds are all equal within experimental error as are the M^+–CH_3 bonds.

In sections 2a and 2b, we present covalent bond models in which either a valence d or s singly occupied orbital on the metal overlaps a singly occupied ligand orbital to form a covalent σ bond (shown in structures II and III, respectively; here +/− refer to orbital

II III

phases).[28] The construction of the metal orbital contribution as either pure d or pure s in character is specifically chosen because it allows us to quantify the resulting periodic σ bond strength trends. The basis of these trends, shown schematically in Figure 5, is that the covalently bound M^+–R molecule does not consist of the two ground-state halves, M^+ and R. Instead, the metal center correlates with an excited $[M^+]^*$ configuration such that the measured bond dissociation energy, D_e, equals the "principal bonding energy," ΔE, diminished by the energetic difference, E_p, between ground-state M^+ and bonding $[M^+]^*$.[29,30] The size of E_p will be estimated and shown to vary according to the metal center and choice of s- vs. d-type bonding. A priori, we expect the character of the bonding in Ru^+, Rh^+, and Pd^+ to differ from that postulated for the first-row transition metals cations. Using a crude estimate for E_p,[31] the intrinsic bond strength, ΔE, of the first-row M^+ was found to be roughly equal to 60 kcal/mol for M^+–H and 70 kcal/mol for M^+–CH_3 (see Figure 6),[2] implying a metal s character covalent bond. Even in this greatly oversimplified picture, the first- and second-row data differ greatly.

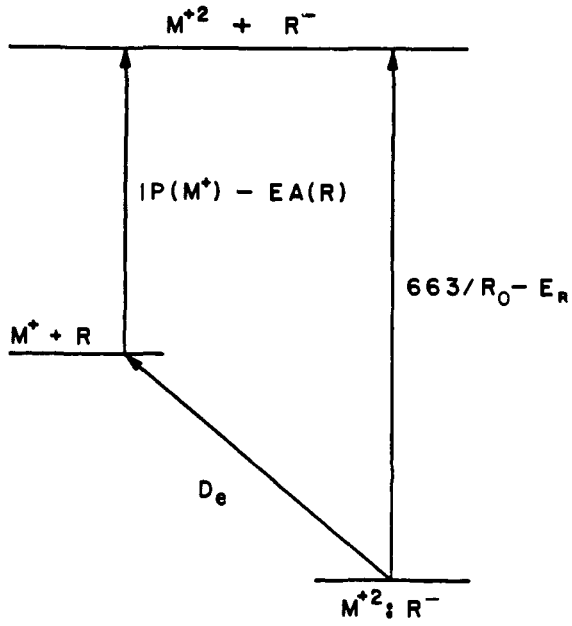

Figure 7. Schematic showing the bonding energy, D_e, expected if M^+–R consists of a M^{2+}–R^- ion pair bound purely by coulombic forces. D_e equals the coulomb energy ($663/R_0 - E_R$) less the energy required to make the ion pair (IP(M^+) − EA(R)) as explained in section 3 of the Discussion.

Lastly, the contribution from ionic bonding will be considered (section 3) in terms of formation of a M^{2+}–R^- ion pair bound by coulombic forces (structure IV; +/− refer to electric charge). The

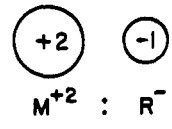

IV

relative contribution of this interaction will depend on the energy differences of the separated ion pairs, M^{2+} and R^-, vs. ground-state M^+ and R (see Figure 7) for Ru^+, Rh^+, and Pd^+ bound to H and CH_3.

1. Metal–Hydrogen vs. Metal–Methyl Bond Strengths: Effects of Polarization of the Ligand. The effects of ligand polarization on the metal–alkyl bonds can be assessed in the limit where the stabilization arises from ion-induced dipole forces. The first-order potential energy term, $V(r)$, of the positive metal ion interaction with the induced ligand dipole is given in eq 4 where R_0 is the

$$V(r) = \frac{-e^2\alpha}{2R^4} = \frac{166\alpha}{R_0^4} \quad \text{(kcal/mol)} \qquad (4)$$

internuclear separation in Å, α is the ligand polarizability in Å^3, and e is the unit charge of the electron.[32] Average values of α are 0.4 and 1.95 Å^3 for H and CH_3 (either planar or pyramidal), respectively.[32,33] Evaluation of eq 4 also requires knowing R_0 for Ru^+, Rh^+, and Pd^+ bound to H and CH_3. Since this information is not directly available, we use the known bond length of Pd–D($X^2\Sigma^+$) of 1.53 Å^3 as an approximation to R_0 for all of the M^{2+}–H^- bond pairs. The similarity in size[34] of M and M^+

(28) Covalency is used in the sense described by L. Pauling in his treatise, "The Nature of the Chemical Bond", Cornell University Press, New York, 1960, Chapter 1.

(29) See ref 28, Chapter 4, for further discussion of this point.

(30) Bonds involving excited *ligand* states are not included in this treatment because they are too high in energy.

(31) E_p was chosen as the minimum $3d^n \rightarrow 4s^13d^{n-1}$ promotion energy for those metal atoms not in a ground-state $4s^13d^{n-1}$ configuration. Electron correlation effects were not treated (infra vide).

(32) S. W. Benson, "Thermochemical Kinetics", Wiley, New York, 1976, pp 185, 310.

(33) J. O. Hirschfelder, C. F. Curtiss, and R. B. Bird, "Molecular Theory of Gases and Liquids", Wiley, New York, 1954, pp 947–951.

(34) Slater shielding constants, S, and calculated ionic radii, r (Å), are respectively for Ru^+(4d) 38.10, 1.43; Rh^+(4d) 38.45, 1.29; Pd^+(4d) 38.80, 1.18; Ru^+(5s) 39.90, 3.23; Rh^+(5s) 40.75, r = 3.11; and Pd^+(5s) 41.60, 3.01: J. E. Huheey, "Inorganic Chemistry", Harper and Row, New York, 1972, pp 40–44; W. A. Goddard III, notes on "The Nature of the Chemical Bond", Vol. II, California Institute of Technology, 1980.

for Ru, Rh, and Pd suggests that this is a reasonable first approximation for these M^{2+}–H^-, but 1.53 Å is surely too small to assign to the M^{2+}–CH_3^- metal–carbon distance. The only recourse available to estimate this latter bond distance is to rely on bond lengths of metal–hydride and metal–methyl groups known for organometallic compounds. Crystallographic studies of many rhodium–hydride and rhodium–methyl organometallics reveal that the average Rh–H bond length is 1.57 Å and the average Rh–CH_3 bond length is 2.08 Å for these complexes,[35,36] about 30% longer. Using this same relative ratio, we assign a nominal value of 2.0 Å to the M^+–CH_3 internuclear separations.

The calculated attractive polarization energies, $V(R_0)$ are 12 kcal/mol for M^+–H and 20 kcal/mol for M^+–CH_3 using the above parameters for Ru^+, Rh^+, and Pd^+. Note that increasing or decreasing the M^+–H or M^+–CH_3 bond lengths by as much as 20%, retaining their relative ratio of about 1:1.3, still produces a polarization energy for M^+–CH_3 that is between 5 and 15 kcal/mol stronger than for M^+–H. Combining this result with the thermochemical data known for saturated complexes, which finds M–CH_3 bonds to be ~15 kcal/mol weaker than M–H bonds, suggests that gas-phase M^+–H and M^+–CH_3 bonds should be roughly *equal* in strength. Reference to Tables IV and V, however, shows that gas-phase cationic metal–methyl bonds are an additional ~10 kcal/mol *stronger* than metal–hydrogen bonds. The small size of the methyl group as well as a comparison of the solution-phase bond strengths of various alkyl groups to metal centers[27] seems to rule out steric factors as the cause of this difference. One possible reconciliation of the gas-phase and solution-phase results may be that the charge-induced polarization of structure I only partially describes the more substantial charge delocalization implied by eq 5. The importance of this resonance

$$M^+–R \leftrightarrow M–R^+ \quad (5)$$

interaction is proportional to the closeness in energy of the two canonical forms, M^+–R and M–R^+.[37] Since the ionization potential of the methyl group (9.8 eV) much more closely matches that for typical transition metals (~7–8 eV) as compared with that for hydrogen (13.6 eV), the $(M–CH_3)^+$ bond will be more resonance stabilized than the $(M–H)^+$ bond. This effect will not occur in solution-phase organometallics where there is an absence of unsolvated charge.[38]

2a. The Covalent Bond Limit, M^+(d)–L. The first covalent bond case is one in which the metal bonding electron is purely d in character and a σ bond results from the overlap of this d orbital with the ligand orbital. Ru^+, Rh^+, and Pd^+ all have high-spin $4d^n$ ground states and have one or more unpaired d electrons available for bonding. Nonetheless, simple division of the M^+(d)–R bonding partners does not correlate diabatically with the ground state of M^+, and the energy, E_p, required to put the metal cations in a bonding configuration can be calculated to a simple approximation. The origins of this energetic difference between M^+ and $[M^+]^*$ (Figure 5) are twofold. First, when an electron in a d orbital on the metal center pairs with the available ligand electron to make a bond, the correlation of the spin of the bonding electron with the spins of the other metal electrons is no longer well defined. Thus, if we simply snap the M^+–R bond and do not allow for relaxation of the metal center, we find that the bonding requirements have forced the metal ion into a $[M^+]^*$ configuration which incorporates both high- and low-spin components and thus is higher in energy than the M^+ ground state. Second, the *atomic* states of the metal cations must be transformed into states for the metal center which will have the appropriate *molecular* symmetry after the bond is formed, i.e., $C_{\infty v}$ for M^+–H and C_{3v} for M^+–CH_3 with the z axis designation chosen as the bonding axis. This, too, has the result of mixing atomic states of higher energy in with the M^+ atomic ground state because the new basis for the molecule frame (we use the familiar d_{z^2}, $d_{x^2-y^2}$, d_{xy}, d_{xz}, and d_{yz} basis) must necessarily be formed from linear combinations of the atomic bases (d_0, $d_{\pm1}$, $d_{\pm2}$). With both of these requirements in mind, we can dress the metal d electrons to prepare for bonding and calculate the difference in energy, E_p, ignoring spin–orbit coupling since it is not significant for the first- and second-row transition metals.[39] In all of the following calculations, the bonding metal electron will occupy the cylindrically symmetric d_{z^2} orbital. This is the only bonding orbital that will satisfy the diatomic symmetry requirements for M^+–H and simplifies the configuration analysis for M^+–CH_3. Developmental work on metal d bonding also suggests that, even in cases without symmetry restrictions, the strongest bonds are formed using the directional d_{z^2}-type orbital and that the energetic difference between a d_{z^2}–R-type σ bond and a d_{xy}-, d_{xz}-, d_{yz}-, or $d_{x^2-y^2}$-type σ bond is roughly 10 kcal/mol or 15% in the overlap.[40,41]

The calculation discussed above is trivial for Pd^+ with its single unpaired d electron and ^2D ground state. The $[M^+]^*$ configuration placing this electron in a d_{z^2} orbital uses one of the microstates of the ^2D ground state, all of which are isoenergetic in the absence of spin–orbit coupling. Therefore, E_p for Pd^+ is zero, and ΔE and D_e are equal in value.

The same calculation becomes more complicated for Rh^+ which has two unpaired d electrons and a ^3F ground state. There are a total of four possible $[M^+]^*$ bonding configurations constrained to have the bonding electron in the d_{z^2}-type orbital: A, ($d_{x^2-y^2}$, d_{z^2}) or (d_{xy}, d_{z^2}); and B, (d_{xz}, d_{z^2}) or (d_{yz}, d_{z^2}) (energetically degenerate configurations are grouped together). Note that the equivalence of electrons and holes produces identical energies and term multiplets for d^n and d^{10-n} configurations which allows d^8 Rh^+ to be discussed in terms of a d^2 configuration.[43] The energy, E_p, of $[M^+]^*$ for each configuration, A and B, above is calculated by transforming these configurations into atomic coordinates and evaluating the relative contribution of various atomic states to the state of $[M^+]^*$. Details of this procedure are given in Appendix IA. The results are listed below where $E(d_i,d_j)$ are the energies of the bonding configurations A (eq 6) and B (eq 7), $E(^{2S+1}L)$

$$(A)\quad E(d_{x^2-y^2},d_{z^2}) = \tfrac{1}{4}\{3E(^3F) + \tfrac{3}{7}E(^1G) + \tfrac{4}{7}E(^1D)\} \quad (6)$$

$$E_p = 7 \text{ kcal/mol}$$

$$(B)\quad E(d_{xz},d_{z^2}) = \tfrac{1}{4}\{\tfrac{6}{5}E(^3F) + \tfrac{6}{7}E(^1G) + \tfrac{1}{7}E(^1D) + \tfrac{9}{5}E(^1P)\} \quad (7)$$

$$E_p = 21 \text{ kcal/mol}$$

are the atomic state energies for Rh^+ and $E_p = E(d_i,d_j) - E(^3F, Rh^+ \text{ ground state})$. All energies used are J-weighted averages for each state.[12] Therefore, the estimated minimum value of E_p for Rh^+ σ bonds is 7 kcal/mol.

Repeating the same procedure for Ru^+ energies requires evaluating the different configurations produced by its three unpaired d electrons. Eliminating all but the lower energy, high-spin possibilities yields three energetically distinct configurations: C, ($d_{x^2-y^2}$, d_{xy}, d_{z^2}); D, ($d_{x^2-y^2}$, d_{yz}, d_{z^2}), (d_{xy}, d_{yz}, d_{z^2}), ($d_{x^2-y^2}$, d_{xz}, d_{z^2}), or (d_{xy}, d_{xz}, d_{z^2}); and E, (d_{xz}, d_{yz}, d_{z^2}).[44] The values of each E_p for these are listed in eq 8–10; see Appendix IA for details.

$$(C)\quad E(d_{x^2-y^2},d_{xy},d_{z^2}) = \{\tfrac{8}{15}E(^4F) + \tfrac{2}{15}E(^4P) + \tfrac{1}{21}E(^2H) + \tfrac{2}{15}E(^2F) + \tfrac{16}{105}E(^2P)\} \quad (8)$$

$$E_p = 18 \text{ kcal/mol}$$

(35) R. G. Teller and R. Bau, "Structure and Bonding," Vol. 44, M. J. Clarke, Ed., Springer Verlag, New York, 1981.
(36) J. P. Collman, P. A. Christian, S. Current, P. Denisevich, T. R. Halbert, E. R. Schmittou, and K. O. Hodgson, *Inorg. Chem.*, **15**, 223 (1976).
(37) G. W. Wheland, "Resonance in Chemistry", Wiley, New York, 1955.
(38) R. H. Crabtree, M. F. Mellea, J. H. Mihekic, and J. M. Quirk, *J. Am. Chem. Soc.*, **104**, 107 (1982).
(39) C. J. Ballhausen, "Introduction to Ligand Field Theory", McGraw-Hill, New York, 1962, Chapter 6.
(40) A. K. Rappé, Ph.D. Thesis, California Institute of Technology, 1981, Chapter 3.
(41) M. L. Steigerwald, Ph.D. Thesis, California Institute of Technology, 1984, Chapter 5.
(42) E. U. Condon and G. H. Shortley, "The Theory of Atomic Spectra", Cambridge University Press, London, 1957.
(43) See ref 39, Chapter 1.
(44) We have ignored symmetry mixing here.

$$(D)\quad E(d_{x^2-y^2},d_{xz},d_{z^2}) = \{{}^{8}/_{15}E(^4F) + {}^{2}/_{15}E(^4P) + {}^{41}/_{420}E(^2H) + {}^{9}/_{70}E(^2G) + {}^{1}/_{30}E(^2F) + {}^{1}/_{14}E(^2D) + {}^{1}/_{420}E(^2P)\} \quad (9)$$

$$E_p = 15 \text{ kcal/mol}$$

$$(E)\quad E(d_{xz},d_{yz},d_{z^2}) = \{{}^{2}/_{15}E(^4F) + {}^{8}/_{15}E(^4P) + {}^{4}/_{21}E(^2H) + {}^{2}/_{15}E(^2F) + {}^{1}/_{105}E(^2P)\} \quad (10)$$

$$E_p = 31 \text{ kcal/mol}$$

Here, $E_p = E(d_i,d_j,d_k) - E(^4F, Ru^+ \text{ ground state})$, the $E(^{2S+1}L)$ are the Ru^+ atomic energies, and the minimum estimated value of E_p for Ru^+ σ bonds is 15 kcal/mol.

Again referring to Figure 5, the phenomenological bond strength, D_e, equals the energy gained from the intrinsic σ overlap of the metal 4d orbital with the ligand orbital, ΔE, *minus* E_p, the energy needed to prepare the metal configuration for the bond. The near equivalence in size of the 4d orbitals[34] suggests strongly that ΔE, the principal σ bond energy, is almost constant for these cations. On this basis, the periodic trend results from variations in E_p for these σ covalent $M^+(d)$–R bonds; the predicted ordering is $D_e(Pd^+–R) > D_e(Rh^+–R) > D_e(Ru^+–R)$ with the sequential decrement equaling 7–8 kcal/mol. This result deviates somewhat from experiment, especially for the M^+–H bond trend.

2b. The Covalent Bond Limit, $M^+(s)$–L. In this case, the bonding electron on the metal center resides in a singly occupied orbital which is purely s in character. Since none of the metal cations Ru^+, Rh^+, or Pd^+ have an electron in a valence 5s orbital in their ground-state configuration, the separation of M^+–R containing a metal s electron in the bond correlates with a linear combination of excited states of M^+. In the "pure s" approximation described above, this $[M^+]^*$ state (see Figure 5) must have a configuration $5s^14d^{n-1}$ and correlates with the atomic states of that designation. Again, we point out that, just as for the covalent d bonding case, both high-spin and low-spin configurations will figure into the description of $[M^+]^*$. Details of this calculation are given in Appendix IB. Therefore, the promotion energy, E_p, required to make metal–s-ligand bonds can be determined from the atomic state splittings of Ru^+, Rh^+, and Pd^+. The values of E_p obtained in this fashion for these three cations are 32 kcal/mol for Ru^+, 60 kcal/mol for Rh^+, and 83 kcal/mol for Pd^+.[12]

The above values of E_p can now be used to assess the trends for the $M^+(s)$–R bond dissociation energies. The 5s orbitals are all very similar in size for Ru^+, Rh^+, and Pd^+,[34] and, as for the case using the 4d orbitals, ΔE in Figure 5 should be very nearly the same for the three metal cations. The predicted trend for this case, then, is that $D_e(Ru^+–R) > D_e(Rh^+–R) > D_e(Pd^+–R)$ with sequential decreases of about 25 kcal/mol. The data in Table III show immediately that this is *not* observed and also that the ΔE for $Pd^+–CH_3$ bond would have to be ~140 kcal/mol—a record single bond strength to any alkyl group found only in a few cases where the bonds are strongly ionic.[45]

3. The Ion Pair Bond Limit: M^{2+}–R^-. The classical inorganic assignment of a −1 charge to H and CH_3 organometallic ligands suggests that it is worthwhile to check the feasibility of ionic bonding between the ion pair M^{2+}–R^-.[46,47] In the limit of purely ion–ion bonding forces, the bond energy of the ion pair is given by eq 11 (see Figure 7). The ion attractive energy term is given

$$D_e(M^{2+}–R^-) = (q_1q_2/R_0) - IP^{II}(M) + EA(R) - E_R \quad (11)$$

by q_1q_2/R_0, where q_1 and q_2 are the ionic charges and R_0 is their separation, $IP^{II}(M)$ is the ionization energy for $M^+ \rightarrow M^{2+}$, EA(R) is the electron affinity of the ligand R (1.8 and 17.4 kcal/mol for CH_3 and H, respectively), and E_R is the Pauli repulsion energy of the electron clouds on the M^{2+} and R^- centers.

Table VI. Estimated Ionic Bond Dissociation Energies for M^{2+}–H^- and M^{2+}–CH_3^-

metal	IP^{II} (eV)[a]	D_e(ionic)[b] M^{2+}–H^- (kcal/mol)	D_e(ionic)[c] M^{2+}–CH_3^- (kcal/mol)
Ru^+	16.76	64	0 (49)
Rh^+	18.07	34	0 (18)
Pd^+	19.42	3	0 (0)

[a] IP^{II} is the energy of $M^+ \rightarrow M^{2+} + e^-$. [b] R_0 taken to be 1.53 Å; see Discussion. [c] R_0 taken to be 2.0 Å (1.53 Å for the number in parentheses); see Discussion.

The results of evaluating eq 11 are tabulated in Table VI; details are given in Appendix II. Since the Pauli repulsion term could not be estimated, it was omitted from the tabulated values, and these must be considered to be *upper bounds* to the actual values at a given R_0.[48] Nonetheless, these crude estimates of the M^{2+}–R^- ionic bond energies differ greatly from the observed experimental data in Table IV. Both of the trends, $D_e(Ru^{2+}–R^-) > D_e(Rh^{2+}–R^-) > D_e(Pd^{2+}–R^-)$ and $D_e(M^{2+}–H^-) >> D_e(M^{2+}–CH_3^-)$, predicted by the ion-pair model contradict the experimental data.

4. Summary. The total bonding picture must be consistent with the two major experimental trends for Ru^+, Rh^+, and Pd^+. (1) All three M^+–H bond strengths are equal within experimental error; the same is true for the three M^+–CH_3 bond energies as well. (2) The M^+–CH_3 bond dissociation energies are all roughly 10 kcal/mol greater than the M^+–H bond dissociation energies. Of the models presented here, the covalent d bonding model and the resonance charge stabilization (ion-induced dipole) model come the closest to accurately predicting trends 1 and 2, respectively. These two bonding types do not cancel or contraindicate each other, and we may describe the M^+–R bonding as a synthesis of both. Moreover, the falloff in bond dissociation energy from Pd^+–R to Ru^+–R of 15 kcal/mol as predicted by the d-type covalent description might be counteracted by the presence of some small amount of s character in the bonding orbital (i.e., the valence metal orbitals s–d hybridize). The M^{2+}–R^- ion pair bonding model can be largely neglected since it is inconsistent with *both* experimental trends and contradicts the charge stabilization model by placing *additional positive* charge on the metal center.

The natures of the M^+–R covalent bonds of Ru^+, Rh^+, and Pd^+ differ from those of the first-row transition metals in that the former have much greater d character. Both theoretical and empirical studies indicate that, for the first-row transition M^+–R series, the metal contribution to the covalent bond is mostly s in character.[2,19] The physical explanation of this discrepancy between the first- and second-row transition metals is probably that the less-well-shielded d orbitals of the first-row metals are much more contracted and do not overlap optimally with incoming ligand orbitals.[19,41]

There have been no published electronic structure calculations for the second-row, group 8 transition metal–hydrogen and –alkyl cations, and the only relevant calculations available for comparison are for neutral PdH.[49–51] While the analogy of PdH to PdH^+ is not straightforward, the theoretical descriptions of the bonding

(45) Examples are the C–F bonds of the freons, the O–H bond in water, and the H–C bond in HCN which lie in the 110–130-kcal/mol range. An excellent compilation is given in D. F. McMillen and D. M. Golden, *Annu. Rev. Phys. Chem.*, **33**, 493 (1982).

(46) J. P. Collman and L. S. Hegedus, "Principles and Applications of Organotransition Metal Chemistry", University Science Books, Mill Valley, 1980.

(47) W. A. Goddard III and L. B. Harding, *Annu. Rev. Phys. Chem.*, **29**, 363 (1978).

(48) There is the distinct possibility that the Pauli repulsion energy for the M^{2+}–H^- is enormous owing to the large average radius of H^- of 1.83 Å which has been calculated to high accuracy by C. L. Pekeris, *Phys. Rev.*, **126**, 1470 (1962).

(49) P. S. Bagus and C. Björkman, *Phys. Rev. A*, **23**, 462 (1981).

(50) P. R. Scott and W. G. Richards, *Chem. Soc. Spec. Period. Rep.*, **4**, 70 (1976).

(51) It may interest the reader to know the other values for Pd–H and Rh–H bonds that have been determined *experimentally* even though it is difficult to compare these quantities directly with our data. (a) The diatomic Pd–H bond dissociation energy is estimated to be 76 kcal/mol: C. Malmberg, R. Scullman, and P. Nylén, *Ark. Fys.*, **39**, 495 (1969). (b) The Rh–H bonds of the three solution-phase complexes of $[P(4\text{-tolyl})_3)_2RhClH_2B]$ (B = (4-tolyl)$_3$, pyridine, and tetrahydrothiophene) have been determined to have an average value 57–58 kcal/mol: R. S. Drago, J. G. Miller, M. A. Hoselton, R. D. Farris, and M. J. Desmond, *J. Am. Chem. Soc.*, **105**, 444 (1983).

in PdH also indicate a strong preference for metal d-type bonding and little partial charge separation.

Conclusions

1. The bond dissociation energies of M^+–CH_3 and M^+–H have been measured for $M^+ = Ru^+$, Rh^+, and Pd^+. The energies for these M^+–R bonds are approximately the same within experimental error for each respective R, with the mean bond dissociation energy equal to 43 kcal/mol for M^+–H and 53 kcal/mol for M^+–CH_3.
2. The periodic trends for these bond energies have been modeled semiquantitatively using simple covalent and electrostatic bonding pictures. Almost certainly, these M^+–R bonds are predominantly covalent in character with the metal contribution to the bond being mostly d-like.
3. The increased M^+–CH_3 bond strength relative to the M^+–H bond by an average 11 kcal/mol is most likely caused by a resonant charge stabilization of the metal cation favored for the more polarizable, more easily ionized methyl ligand. Contributions from M^{2+}–R^--type structures appear to be unimportant.
4. More sophisticated theoretical treatments will undoubtedly reveal additional subtleties about the nature of these M^+–R bonds but are expected to be consistent with the overall predictions of our empirically derived model.

Acknowledgment. M.L.M. wishes to thank Dr. M. L. Steigerwald for many helpful discussions about the theoretical calculations and the Bantrell Foundation for a California Institute of Technology Bantrell Fellowship. Graduate fellowship support from Bell Laboratories and SOHIO, in addition to postdoctral support from EXXON, is gratefully acknowledged by L.F.H.

Appendix I

A. The calculation of the energy, E_p, of configuration D for Ru^+ will be used as an example. This can be accomplished either of two ways. The first way takes the wave function for D, transforms it into atomic coordinates, and projects this onto the atomic state wave functions. For configuration D, the wave function is given by eq A1 where α and β are the spin functions.

$$\Psi_{Ru^{+*}(D)} = \frac{1}{\sqrt{2}}\Psi_{core}\{\Psi(d_{x^2-y^2},d_{xz},d_{z^2})(\alpha\alpha\alpha) + \Psi(d_{x^2-y^2},d_{xz},d_{z^2})(\alpha\alpha\beta)\} \quad (A1)$$

Neglecting the core, and transforming the real orbitals $d_{x^2-y^2}$, d_{xz}, and d_{z^2} into the complex orbitals $d_{\pm2}$, $d_{\pm1}$, and d_0 gives $\Psi_{Ru^{+*}(D)}$ of eq A2 where d_{+2} is denoted by 2, d_{-2} is denoted by $\hat{2}$, etc.

$$\Psi_{Ru^{+*}(D)} = \frac{1}{\sqrt{2}}\left\{\Psi\left(\frac{2+\hat{2}}{\sqrt{2}},\frac{1+\hat{1}}{\sqrt{2}},0\right)\times(\alpha\alpha\alpha) + \Psi\left(\frac{2+\hat{2}}{\sqrt{2}},\frac{1+\hat{1}}{\sqrt{2}},0\right)(\alpha\alpha\beta)\right\} \quad (A2)$$

Expanding this wave function and dropping the "Ψ" yields eq A3 ($\alpha \equiv +$, $\beta \equiv -$). Next, we take $\Psi_{Ru^{+*}}$ from (A3) and transform

$$\Psi_{Ru^{+*}(D)} = \frac{1}{2\sqrt{2}}\{(2^+,1^+,0^+) + (2^+,\hat{1}^+,0^+) + (\hat{2}^+,1^+,0^+) + (\hat{2}^+,\hat{1}^+,0^+) + (2^+,1^+,0^-) + (2^+,\hat{1}^+,0^-) + (\hat{2}^+,1^+,0^-) + (\hat{2}^+,\hat{1}^+,0^-)\} \quad (A3)$$

it once again using a new basis set composed of the d^3 atomic state wave functions. This is done by taking the overlap of the wave function in (A3) with the orthonormal set of wave functions for the atomic states (written as $\psi(L,M_L,S,M_S)$ below) of Ru^+ which is d^3;[52] see equation A4. The wave functions for each of the atomic

(52) Many of these can be found in ref 42, pp 227–228; the authors will furnish missing ones on request.

$$\begin{aligned}\langle\Psi_{Ru^{+*}(D)}|\sum_i\Psi(^4F,^4P,^2H,^2G,^2F,^2_{\pm}D,^2P)\rangle = \\ \frac{1}{2\sqrt{2}}\Big\{[\Psi(3,3,3/2,3/2) - \Psi(3,-3,3/2,3/2) - \\ \frac{\sqrt{3}}{\sqrt{5}}\Psi(3,1,3/2,3/2) + \frac{\sqrt{3}}{\sqrt{5}}\Psi(3,-1,3/2,3/2) + \\ \frac{1}{\sqrt{3}}\Psi(3,3,3/2,1/2) - \frac{1}{\sqrt{3}}\Psi(3,-3,3/2,1/2) - \\ \frac{\sqrt{3}}{\sqrt{15}}\Psi(3,1,3/2,1/2) + \frac{\sqrt{3}}{\sqrt{15}}\Psi(3,-1,3/2,1/2)] + \\ \Big[-\frac{\sqrt{2}}{\sqrt{5}}\Psi(1,1,3/2,3/2) + \frac{\sqrt{2}}{\sqrt{5}}\Psi(1,-1,3/2,3/2) - \\ \frac{\sqrt{2}}{\sqrt{15}}\Psi(1,1,3/2,1/2) - \frac{\sqrt{2}}{\sqrt{15}}\Psi(1,-1,3/2,1/2)\Big] + \\ \Big[-\frac{\sqrt{2}}{\sqrt{15}}\Psi(5,3,1/2,1/2) + \frac{\sqrt{2}}{\sqrt{15}}\Psi(5,-3,1/2,1/2) - \\ \frac{\sqrt{54}}{\sqrt{210}}\Psi(5,1,1/2,1/2) + \\ \frac{\sqrt{54}}{\sqrt{210}}\Psi(5,-1,1/2,1/2)\Big] + \Big[-\frac{3}{\sqrt{20}}\Psi(4,3,1/2,1/2) - \\ \frac{3}{\sqrt{20}}\Psi(4,-3,1/2,1/2) - \frac{3}{\sqrt{140}}\Psi(4,1,1/2,1/2) + \\ \frac{3}{\sqrt{140}}\Psi(4,-1,1/2,1/2)\Big] + \\ \Big[\frac{1}{\sqrt{12}}\Psi(3,3,1/2,1/2) - \frac{1}{\sqrt{12}}\Psi(3,-3,1/2,1/2) + \\ \frac{1}{\sqrt{20}}\Psi(3,1,1/2,1/2) - \frac{1}{\sqrt{20}}\Psi(3,-1,1/2,1/2)\Big] + \\ \Big[-\frac{2}{\sqrt{14}}\Psi_-(2,1,1/2,1/2) + \frac{2}{\sqrt{14}}\Psi_-(2,-1,1/2,1/2)\Big] + \\ \Big[-\frac{1}{\sqrt{105}}\Psi(1,1,1/2,1/2) + \frac{1}{\sqrt{105}}\Psi(1,-1,1/2,1/2)\Big]\Big\} \end{aligned} \quad (A4)$$

states have been bracketed together in eq A4 for ^4F, ^4P, ^2H, ^2G, ^2F, $_-{}^2D$, and ^2P, respectively; note that there are no cross terms in $^2_{\pm}D$. Now, the energy of the $\Psi_{Ru^{+*}(D)}$, given in eq A5, can be

$$E_p = \frac{\langle\Psi_{Ru^{+*}(D)}|\hat{H}|\Psi_{Ru^{+*}(D)}\rangle}{\langle\Psi_{Ru^{+*}}|\Psi_{Ru^{+*}}\rangle} \quad (A5)$$

determined easily since for all of the orthonormal atomic wave functions, this quantity in eq A6 equals the energy of the ith atomic

$$\langle\Psi_i(L_i,M_{L_i},S_iM_{S_i})|\hat{H}|\Psi_j(L_j,M_{L_j},S_j,M_{S_j})\rangle \quad (A6)$$

state for $i = j$ and equals zero for $i \neq j$ (recall that in the absence of L–S coupling the microstates of any atomic state are energetically degenerate).[39] The result of eq A5 for the wave function in (A4) is given in eq 9 in the main text.

An alternative method of doing this calculation involves writing the energy of the wave function in eq A2 and the ground state in terms of the coulomb, J, and exchange, K, integrals so as to evaluate E_p.[47] This is shown in eq A7–A9, using configuration

$$E\left[(d_{x^2-y^2},d_{xz},d_{z^2})\left(\alpha\alpha,\frac{\alpha+\beta}{\sqrt{2}}\right)\right] = J_{12} + J_{20} + J_{10} - \frac{1}{2}(K_{12} + K_{\bar{1}2} + K_{20} + K_{10}) \quad (A7)$$

$$E(^4F) = J_{12} + J_{20} + J_{10} - K_{12} - K_{10} - K_{20} \quad (A8)$$

$$E(d_{x^2-y^2},d_{xz},d_{z^2}) - E(^4F) = E_p(D) = \frac{1}{2}(K_{12} + K_{10} + K_{20} - K_{\bar{1}2}) \quad (A9)$$

D as an example. The values of these J and K integrals can be determined from the integrals of the Legendre functions, F, and atomic state splittings,[42,43] e.g., $K_{12} = 6F_2 + 5F_4$ where F_2 and F_4 are reckoned from empirical data.[42,43] This method is much more tractable for d^4-, d^5-, s^1d^n-, etc., type configurations than the method described in the previous paragraph but requires knowing how to express the energy of wave functions in terms of the J and K integrals as in eq A7 and A8. The value of E_p reached by both procedures will be the same.

B. The calculation of E_p for $Pd^+4d^9 \rightarrow 5s^14d^8$ will be shown as an example. As pointed out in Appendix IA, the method using energies expressed as sums of exchange and coulomb integrals is much more straightforward than the alternative method and will be used for evaluating E_p here.

The wave functions for $Pd^+(^4F)$ and $Pd^+(^2F)$, the lowest two states of the $5s^14d^8$ configuration, are given in eq A10 and A11

$$\Psi_{Pd^+}(^4F) = \Psi_{core}\Psi(S,2,1)(\alpha\alpha\alpha) \quad (A10)$$

$$\Psi_{Pd^+}(^2F) = \Psi_{core}\Psi(S,2,1)(\beta\alpha\alpha) \quad (A11)$$

and the bonding wave function for Pd^{+*} is shown in eq A12 where

$$\Psi_{Pd^{+*}}(5s^14d^8) = \frac{1}{\sqrt{2}}\Psi_{core}\{\Psi(s,d_{x^2-y^2},d_{xz})(\alpha\alpha\alpha) + \Psi(s,d_{x^2-y^2},d_{xz})(\beta\alpha\alpha)\} \quad (A12)$$

$l = 2$, $m_1 = 2$ and 1 are expressed as "2" and "1", and $l = 0$, $m_1 = 0$ is expressed as "s". Writing $\Psi_{Pd^{+*}}$ in terms of the complex atomic orbitals gives eq A13. The energies of each of these wave

$$\Psi_{Pd^{+*}}(5s^14d^8) = \frac{1}{\sqrt{2}}\left[\Psi\left(s,\frac{2+\hat{2}}{\sqrt{2}},\frac{1+\hat{1}}{\sqrt{2}}\right)\times(\alpha\alpha\alpha) + \Psi\left(s,\frac{2+\hat{2}}{\sqrt{2}},\frac{1+\hat{1}}{\sqrt{2}}\right)(\beta\alpha\alpha)\right] \quad (A13)$$

functions in terms of the J's and K's are listed in eq A14–A16.

$$E[\Psi_{Pd^+}(^4F)] = J_{S2} + J_{S1} + J_{12} - K_{S2} - K_{S1} - K_{12} \quad (A14)$$

$$E[\Psi_{Pd^2}(^2F)] = J_{S2} + J_{S1} + J_{12} + K_{S2} + K_{S1} - K_{12} \quad (A15)$$

$$E[\Psi_{Pd^{+*}}(5s^14d^8)] = J_{S2} + J_{S1} + J_{21} - \tfrac{1}{2}(K_{12} + K_{\bar{1}2} + K_{S2} + K_{S1}) \quad (A16)$$

The difference between the energies of the ^4F and ^2F states gives a value, eq A17, which yields the energy of the $Pd^{+*}(5s^14d^8)$ bonding configuration in simple terms, eq A18. From the J-weighted average energies of $Pd^+(^4F)$ and $Pd^+(^2F)$ states and the values of $K_{\bar{1}2}$ and K_{12} which are determined as described in Appendix IA, we obtain $E_p = E[\Psi_{Pd^{+*}}(5s^14d^8)] = 83$ kcal/mol; note that this is about 9 kcal/mol higher than the simple average $4d^9(^2D) \rightarrow 5s^14d^8(^4F)$ splitting of about 74 cal/mol.[12]

$$E_{DIFF} = E[\Psi_{Pd^+}(^2F)] - E[\Psi_{Pd^+}(^4F)] = 2(K_{S2} + K_{S1}) \quad (A17)$$

$$E[\Psi_{Pd^{+*}}(5s^14d^8)] = E[\Psi_{Pd^+}(^4F)] + \frac{1}{4}E_{DIFF} - \frac{1}{2}(K_{\bar{1}2} - K_{12}) \quad (A18)$$

Appendix II

The origin of eq 11 can be seen directly from the thermodynamic cycle in eq A19 and A20, where the attractive energy,

$$\begin{array}{ccccc} M^{2+}-R^- & \xrightarrow{D_e} & M^+ + R & & \\ \downarrow q_1q_2(R_0-E_R) & & & \uparrow -IP^{II}(M) & \\ M^{2+} + R^- & \xrightarrow[+EA(R)]{} & M^{2+} + R + e^- & & \end{array} \quad (A19)$$

$$D_e = \frac{663}{R_0} - E_R - IP^{II}(M) + EA(R) \text{ (kcal/mol)} \quad (A20)$$

q_1q_2/R_0, has been diminished by the Pauli repulsion energy, E_R. The origin of this repulsion term lies in the Pauli exclusion principle, and determination of its magnitude requires a much more sophisticated theoretical treatment beyond the scope of our approach. Therefore, we will present D_e where E_R is not explicitly included. The approximations of R_0 for the metal–methyl and metal–hydrogen internuclear separations are explained in the Discussion, section 1; the same values of 1.53 and 2.0 Å, respectively, are used here as well.

The ionic bonding between the alternative ion pair, M^-–R^{2+}, is not considered since it is impossible for R = H and highly unlikely for $R = CH_3$ where the energy required to doubly ionize $CH_3 \rightarrow CH_3^{2+} + 2e^-$ is enormous, about 36 eV,[53] as compared with typical values of 25 eV for $M \rightarrow M^{2+} + 2e^-$ (see eq A18). Lastly, higher multipole terms between either M^{2+}–R^- or M^-–R^{2+} are much smaller in magnitude than the $1/R$ ion–ion forces and can be neglected.

Registry No. $RuCD_3^+$, 90624-33-2; $RhCD_3^+$, 90641-25-1; $PdCD_3^+$, 90624-34-3; Fe^+-H, 71899-96-2; Fe^+-CH_3, 90143-29-6; Co^+-H, 12378-09-5; Co^+-CH_3, 76792-06-8; Ni^+-H, 75181-25-8; Ni^+-CH_3, 90624-35-4; Ru^+-H, 90624-36-5; Ru^+-CH_3, 90624-37-6; Rh^+-H, 90624-38-7; Rh^+-CH_3, 90624-39-8; Pd^+-H, 85625-94-1; Pd^+-CH_3, 90624-40-1; Mn^+-H, 75641-96-2; Mn^+-CH_3, 89612-54-4; RuD^+, 90624-41-2; RhD^+, 90624-42-3; PdD^+, 90624-43-4; η^5-$CpRh(CO)_2$, 12192-97-1; Ru^+, 20019-76-5; Rh^+, 20561-59-5; Pd^+, 20561-55-1; C_2D_6, 1632-99-1; D_2, 7782-39-0; C_2H_6, 74-84-0.

(53) This number is derived from the sum of the vertical ionization potential for $CH_3 \rightarrow CH_3^+ + e^-$ (=9.8 eV) and the Hartree–Fock calculated value for the vertical ionization potential for $CH_3^+ \rightarrow CH_3^{2+} + e^- \approx 26$ eV: M. L. Steigerwald, unpublished results.